Performance Analysis of Outer Rotor Wound Field Flux Switching Machine for Direct Drive Application

N. Ahmad [1], F. Khan [1], N. Ullah [1,2], and M. Z. Ahmad [3]

[1] Department of Electrical Engineering
COMSATS Institute of Information and Technology, Abbottabad, Pakistan
n.ahmadmwt@gmail.com, faisalkhan@ciit.net.pk

[2] U.S.-Pakistan Center for Advanced Studies in Energy
University of Engineering & Technology, Peshawar, Pakistan

[3] Research Center for Applied Electromagnetics
Universiti Tun Hussein Onn Malaysia, Locked Bag 101, BattuPahat, Johor, 86400 Malaysia
zarafi@uthm.edu.my

Abstract ─ One of the premium in-wheel applications is direct drive, evolving enormously for HEV's. An alternative and lot of research especially on the outer rotor field excitation flux switching machine is required to overcome the problems like demagnetization and high cost of rare earth magnetic material used in interior permanent magnet synchronous machine (IPMSM). Salient rotor pole and non-overlapping winding embedded in electrical machine design possess some pertinent features such as; reduce copper losses, low-cost, and usage in high speed applications. Therefore, this paper emphasizes on the design of three-phase outer rotor wound field FSM employing optimization, performance analysis and MEC models of proposed 12-slot/13-pole FSM corresponding to different rotor positions are combined as GRN and are solved utilizing incidence matrix methodology using MATLAB. Moreover, FSM flux behavior, no-load, and load analysis were examined using JMAG software and based on FEA. Results obtained from GRN methodology and corresponding FEA results close resemblance with and errors less than ~1.2%, hence validating accuracy of GRN methodology. The proposed design for hybrid electric vehicle torque characteristic is compared with existing IPMSM and 6-slot/7-pole non-overlapping stator wound flux switching machine (NSWFS).

Index Terms ─ Deterministic optimization, flux switching machine, HEV's, outer rotor, MEC.

I. INTRODUCTION

Electric and hybrid electric vehicles are used to minimize environmental pollution and reduce usage of fossil fuels. HEV is an ideal solution to control global warming, reduce energy crisis, and minimize CO_2 emission [1]. Due to increased consumption of fossil fuels, their reservoirs are going down and price is going up. HEV is attracting interests of research community and automobile industry due to its unique property of utilizing electrical power (Batteries, Fuel Cells, etc.). Design of electric motor drives for EVs must show characteristics of high power density, high torque at low speed, quick torque response, high robustness, low torque ripples and noise, reliability, constant power at high speed and cost effective [2]-[3].

Design and structure of Flux Switching Machine (FSM) resembles with doubly salient permanent magnet machine [4]-[5], combining features of Permanent Magnet Machine and Switched Reluctance Machine. Flux sources (Permanent Magnet or Field Excitation Coil and Armature Winding) are confined to stator, leaving rotor completely passive. Due to this unique topology FSM is suited for high speed applications. FSM are categorized as Field Excited FSM (FEFSM), Permanent magnet FSM (PMFSM), and Hybrid Excited FSM (HEFSM). PMFSM and FEFSM comprise of FEC and PM respectively as their major flux sources whilst PM and FEC both are reasons for flux sources for HEFSM [6]-[7]. PMFSM comprise of rare earth magnet material and exhibits high efficiency and high torque density depending upon the type of material [8]-[9]. PM have drawbacks such as less robust, costly, reduction of flux density due temperature rises and time span. After discovery of rare earth PM material, it attracted interest of research community and industries.

To overcome the above-mentioned obstacles, the three phase non-overlapping field wound winding FSM with twenty-four teeth stators (12 slots for armature and 12 slots for field winding) is discussed in [10]. Model discussed [11] inner rotor non-overlapping stator wound

field synchronous machine that incorporated minimum torque ripple and high torque density. The inner rotor machine can belt with combustion engine. Outer rotor FEFSM used in HEV in wheel have advantages to eliminate mechanical transmission, drive belts, and differential gears and has high efficiency, increased vehicle space, and weight reduction [12].

ORFEFSM received attention of designers in the recent past and a lot of research is carried out in this field. Magnetic Equivalent Circuits (MEC) modeling, Finite Element Analysis (FEA) and Fourier Analysis (FA) are popular designing methodologies. MEC models with Reluctance Network Method (RNM) topology are preferred over other two methods due to disadvantages of FEA (computational complexity) and FA (less accuracy).

This paper emphasizes on the design of three-phase outer rotor wound field FSM employing salient rotor pole and non-overlapping winding. The profile of flux linkage and verified by MEC model and GRN network. Moreover, flux linkage, copper losses, iron losses, and efficiency versus current density are analyzed on 2D FEA. This study employing deterministic optimization in the enhancement of average torque, compared to existing IPM and 6-slot\7-pole NSWFS machines.

II. DESIGN METHODOLOGY

The basic principle of FEFSM depends upon the position of rotor because magnetic flux linkage may be either negative or positive in the armature winding with respect to the rotor position while stator, armature and excitation coil are stationary. Figure 1 illustrates the cross-sectional view of machine and design parameters are demonstrated in Table 1. The performance parameters of the proposed design are comparatively lower than wound field flux switching machine discussed in [13], [14]. The proposed motor 12-slot/ 13-pole ORFEFSM, in order to enhance the average electromagnetic torque characteristic, deterministic optimization technique is carried out. The magnetic flux distribution of un-optimized and optimized design depicts in Fig. 3.

In deterministic optimization back iron length, rotor pole width, stator pole width, and stator slot (FEC and armature) are consider as optimal free variables, and the optimal objective is electromagnetic torque. Firstly, change the rotor parameters (rotor pole width and length) while keeping constant all stator parameters to achieve optimal torque.

A. Optimization procedure

The proposed 12-slot/13-pole outer rotor FEFSM is optimized to enhance the torque characteristic. The initial torque achieved is 88.04 Nm, while the target torque 138 Nm. To achieve better performance, the rotor and stator parts have design parameters S1 to S7, as shown in Fig. 2 (a).
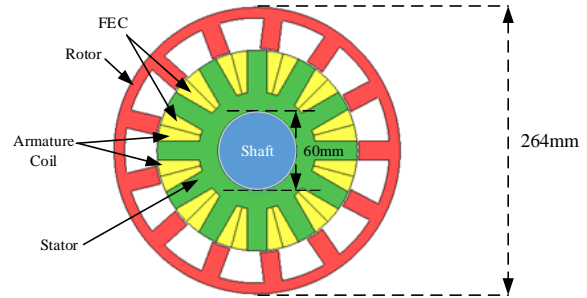

Fig. 1. Cross section of 12S/13P.

Table 1: Design parameters and comparison

Design Parameter	Un-Optimized	Optimized	IPM	NWFS
Number of stator slot	12	12	48	6
Number of rotor pole	13	13	8	7
Axial length (mm)	50.8	50.8	50.8	132
Stator outer diameter (mm)	132	132	132	50.8
Air gap(mm)	0.73	0.73	0.73	0.73
Split ratio	0.7	0.82	0.61	0.66
Stator tooth width (mm)	20	24	7.3	33.5
Back iron (mm)	9	10	20.2	17.5
Rotor pole arc (degree)	--	---	--	21.0
Rotor pole width	18	20	--	--

S1 and S2 are the rotor parameters, S3 is the radius of the stator, S4 is back iron of stator, S5 and S6 are the stator poles width, and S7 is armature coil parameter. Whereas, S1 and S2 are the depth and width of rotor pole, respectively. Deterministic optimization technique is applied to achieve targets requirements. In deterministic optimization technique, the air gap and slot area of armature coil and FEC are kept constant while a free parameter is changed. Firstly, change the rotor parameters S1 and S2 while keeping all free parameters of the stator constant. In order to accomplish maximum torque, rotor pole depth, S1 and rotor pole width, S2 are changed while other parameters are kept constant. Moreover, S3 is the most dominant parameter for attaining maximum torque and is updated as follows. Increasing the stator radius S3 will result in increasing the stator back iron length S4, while keeping armature slot area S7 and FEC slot area S6 constant. Once the maximum torque is achieved, the stator radius S3 and S4 are kept constant and S5, S6 and S7 are changed. Similarly, the optimal S5 value is also kept constant and S6 is updated. The torque improvements are shown in Fig. 2 (b).

Secondly, keeping constant rotor parameters and altering stator parameters (stator back iron length, stator

pole width, and stator slots). This process repeated up to three times to achieve maximum torque. The design optimization process and modification is reiterated until the maximum torque performance is achieved. After optimization process, the structure difference between initial and final design, as illustrated in Fig. 3. Moreover, the armature slot of final design has 29.93% higher depth than FEC slot to produce optimal magnetic flux.
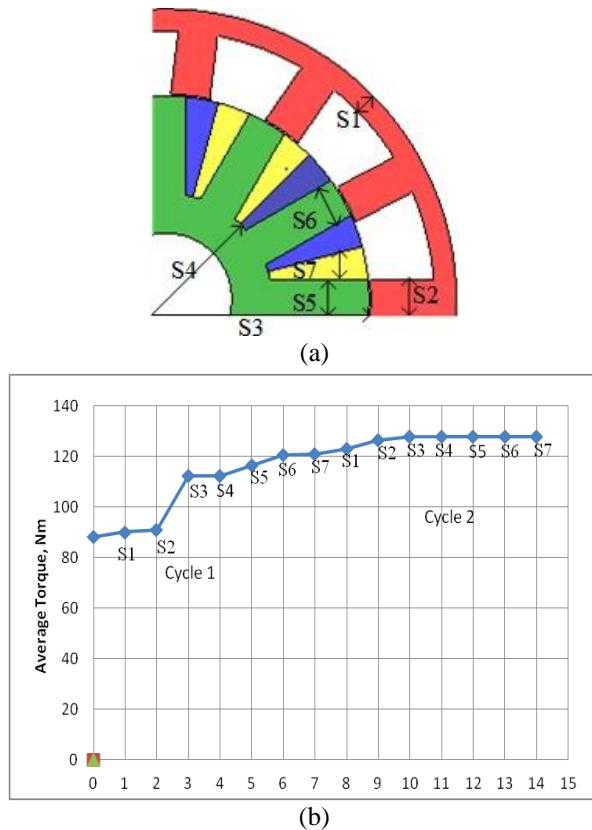

(a)

(b)

Fig. 2. (a) Design parameter for optimization; (b) average torque effect on different parameters.

(a) Un-optimized   (b) Optimized
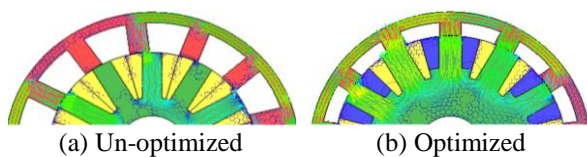
Fig. 3. The structure difference between initial and final design: (a) un-optimized and (b) optimized.

III. PERFORMANCE ANALYSIS

A. Coil test analysis

The operation principle of outer rotor FEFSM for HEV application is verified by coil arrangement test and investigating the magnetic flux linkage in each armature coil slot. Then a DC is supplied to FEC while AC is supplied to armature coils at maximum current density.

Figure 4 illustrated the position of armature coil and Table 2 depicts combination of armature coil. The conventional three phase system simulated by 2D FEA using JMAG designer is represented by U, V, and W respectively as shown in Fig. 5. The direction of FEC coil is clockwise. The coil test is performed on no load condition and observed the magnetic flux linkage. The three phase flux linkage is verified by Magnetic Equivalent Circuit (MEC) as below discussed.

Table 2: Armature coil phase representation

Phases	Armature Coil
U	A1, A2, A7, A8
V	A5, A6, A11, A12
W	A3, A4, A9, A10

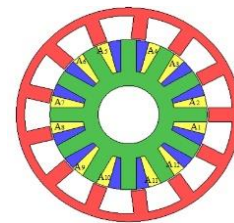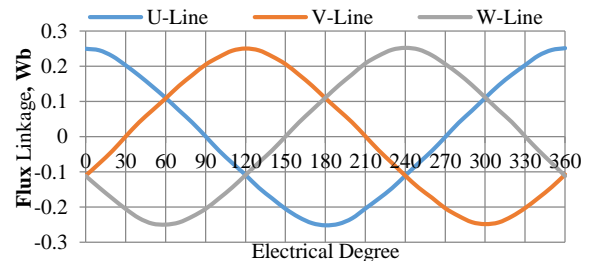Fig. 4. Position of armature coil.

Fig. 5. Three phase flux linkage.

1) Magnetic equivalent circuit modules

Reluctance networks of 12slot/13pole ORFEFSM air gap magnetic equivalent circuit modules corresponding to different rotor positions, rotor magnetic equivalent circuit modules and stator magnetic equivalent circuit modules are combined as Global Reluctance Network (GRN). To avoid computational complexity, half machine is modeled under different segments corresponding to rotor position. Air gap flux distribution mainly contribute to performance of ORFEFSM, as conversion of electrical machine energy takes place in this medium. Air gap MEC modules are sensitive to rotor tooth position, each MEC module repeats itself after specified rational position which suggest possibilities of reducing verities of GRN.

As the rotor position changes, air gap flux paths or flux tubes changes resulting in changed flux tube permeance and also flux concentration. Area that encloses

flux lines is defined as flux tubes [15]. To reduce errors and uplift accuracy of GRN, flux tubes permeance must be calculated accurately. Flux tubes for different rotor positions were analyzed based on position state shifting and concluded about periodic nature as these flux tubes are repeated, therefore half machine model is investigated. Various combinations of air gap magnetic equivalent circuit modules corresponding to different rotor positions are implemented, variation of air gap flux distribution is expressed as series of MEC modules and is termed as GRN.

Figure 6 (a) and Fig. 6 (c) shows flux tubes having identical lengths of flux lines. Equation (1) is used to calculate total reluctance (R) of flux tube as a line integral through the curve:

$$R = \int_l \frac{1}{\mu A} dl. \tag{1}$$

Where, μ is material's permeability, l is curve of enclosed flux lines, dl length element through l, and A is area of the face perpendicular to l. Both A and μ may vary through the curve l.

Figure 6 (b) and Figs. 6 (d-f) shows the flux tubes having different lengths of flux lines and identical cross-section faces. Equation (2) is used to calculate total permeance (P) of flux tube as a surface integral over the head face of this tube:

$$P = \iint_A \frac{\mu}{l} dA. \tag{2}$$

2) Air Gap MEC modules

FEA on 13/12 ORFEFSM is performed to model air gap magnetic flux distribution when rotor tooth travels in different segments. Where, A, dA, l, and μ are head face of flux tube, surface element on the head face, total length of a flux line originated from one face element, and material's permeability, respectively. Both l and μ can change over surface A. Six types of flux tubes are used in this paper (as shown in Fig. 6) and their respective permeance (P) calculation formulas are shown in Table 3. X-axis of flux tubes show flux paths (equally distributed lines) and Y-axis represents magnetic properties of each flux path (assumed to be homogenous). Figure 6 (a) and Fig. 6 (b) shows two types of flux tubes and their permeance calculations are done using cylindrical coordinate system to reduce computational complexity, while Figs. 6 (c-f) flux tubes permeance calculations are done using Cartesian coordinate system.

FEA are grouped into certain number of flux tubes as shown in Fig. 7 (a) (interval 1), Fig. 8 (a) (interval 2), Fig. 9 (a) (interval 3), Fig. 10 (a) (interval 4) and Fig. 11 (a) (interval 5). Figure 6 represents different types of flux tubes selected from Table 3 for permeance calculations. Permeance calculation for each flux tube is done by using equations introduced in Table 3. Five different

airgap MEC modules with variable permeances are shown in Fig. 7 (b) (interval 1), Fig. 8 (b) (interval 2), Fig. 9 (b) (interval 3), Fig. 10 (b) (interval 4) and Fig. 11 (b) (interval 5) as shown in Table 4. Multiple parallel permeances are reduced to single branch permeance and four different topologies are presented in Fig. 7 (c) (interval 1), Fig. 8 (c) (interval 2), Fig. 9 (c) (interval 3), Fig. 10 (c) (interval 4) and Fig. 11 (c) (interval 5).
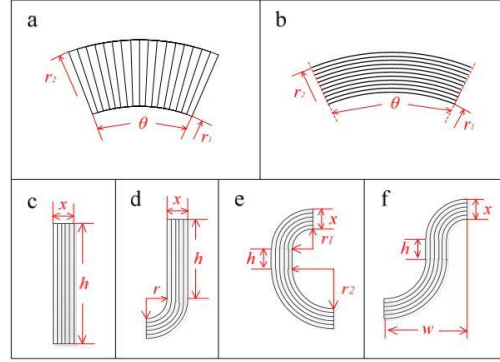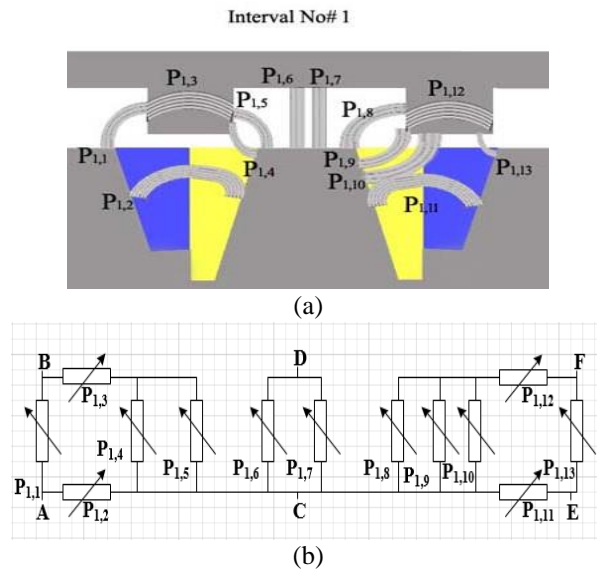

Fig. 6. Flux tubes.

Table 3: Formulas

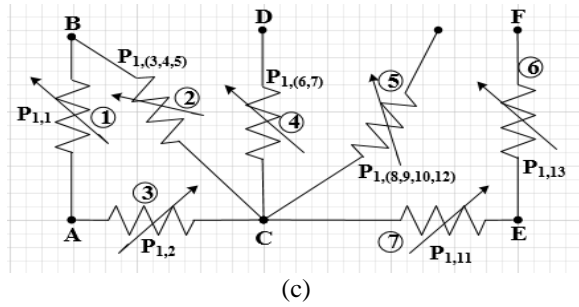| Flux Tubes	Permeance (*P*)	Flux Tubes	Permeance (*P*)
a	$\dfrac{\mu L\theta}{\ln(\frac{r_2}{r_1})}$	d	$\dfrac{2\mu L.\ln\left(1 + \frac{\pi x}{\pi r + 2h}\right)}{\pi}$
b	$\dfrac{\mu L\ln(\frac{r_2}{r_1})}{\theta}$	e	$\dfrac{\mu L.\ln(1 + \frac{2\pi x}{\pi r_1 + \pi r_2 + 2h})}{\pi}$
c	$\dfrac{\mu L x}{h}$	f	$\dfrac{2\mu L x}{(\pi w + 2h)}$

Interval No# 1

(a)

(b)

Fig. 7. Air gap MEC Module 1: (a) flux tubes corresponding to rotor tooth for interval No. 1, (b) detailed MEC, and (c) MEC topology.
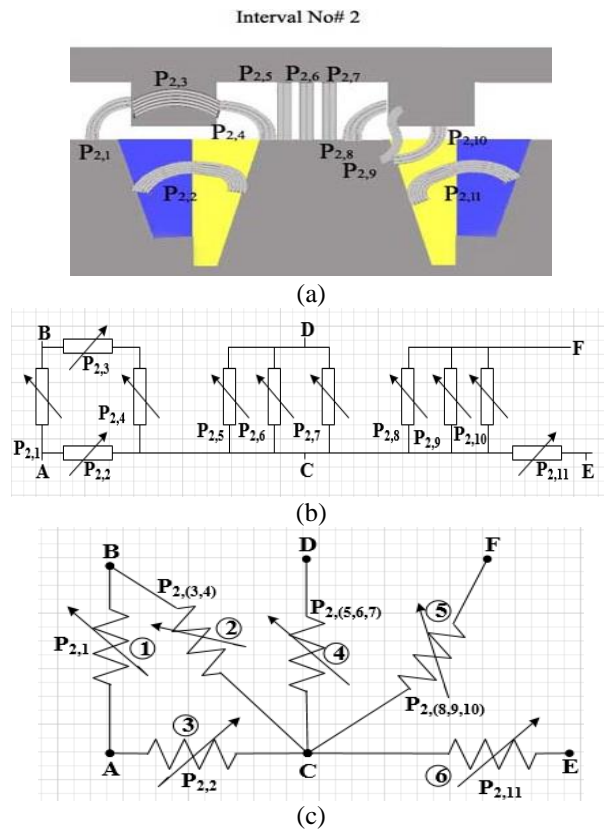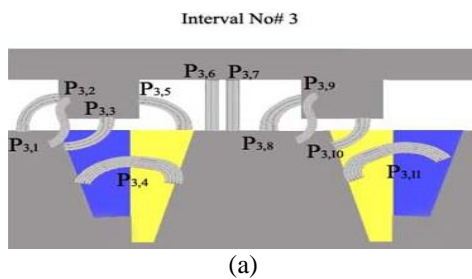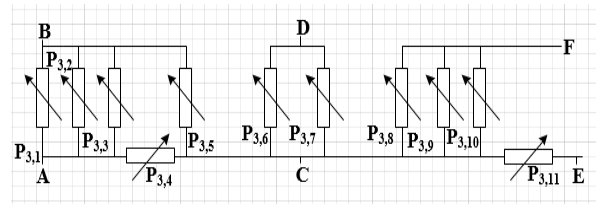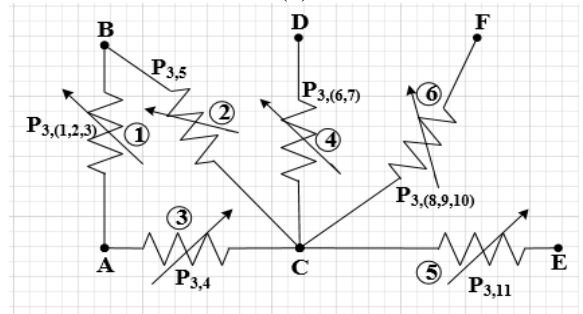

Fig. 8. Air gap MEC Module 2: (a) flux tubes corresponding to rotor tooth for interval No. 2, (b) detailed MEC, and (c) MEC topology.

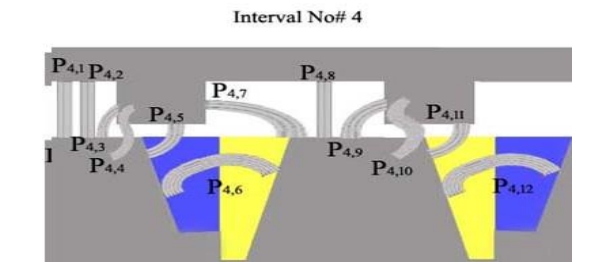Fig. 9. Air gap MEC Module 3: (a) flux tubes corresponding to rotor tooth for interval No. 3, (b) detailed MEC, and (c) MEC topology.

Fig. 10. Air gap MEC Module 4: (a) flux tubes corresponding to rotor tooth for interval No. 4, (b) detailed MEC, and (c) MEC topology.

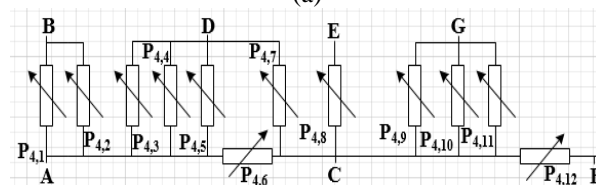Fig. 11. Air gap MEC Module 5: (a) flux tubes corresponding to rotor tooth for interval No. 5, (b) detailed MEC, and (c) MEC topology.
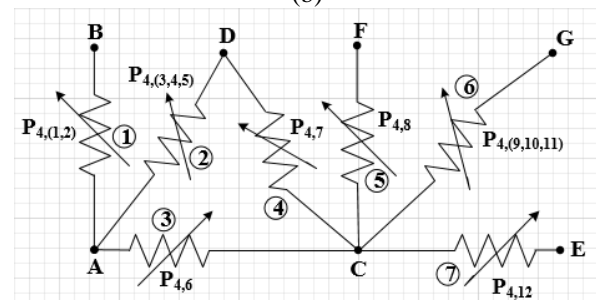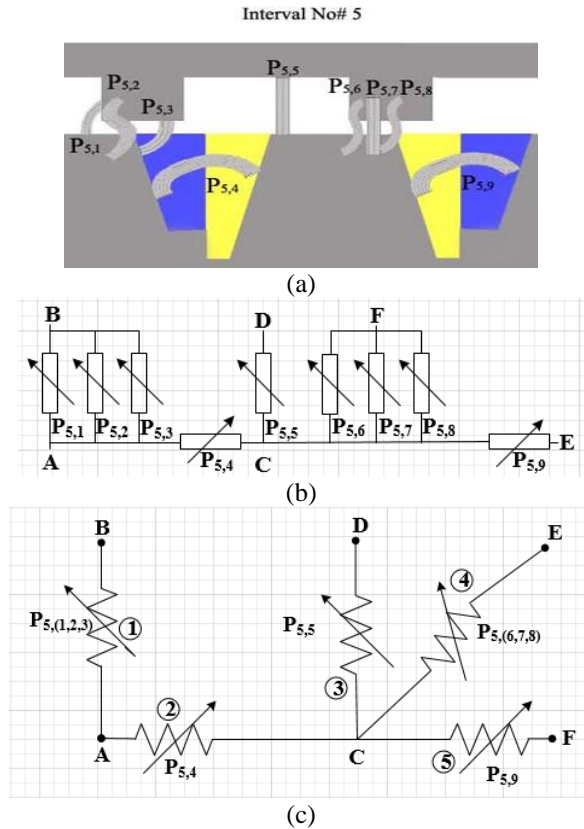
Table 4: Flux tubes in different air gap MEC Modules

Flux Tube Number	1	2	3	4	5	6	7	8	9	10	11	12	13
P1,j	D	E	B	D	D	C	C	D	D	D	E	B	D
P2,j	D	E	B	D	C	C	C	D	F	D	E	-	-
P3,j	D	F	D	E	D	C	C	D	F	D	E	-	-
P4,j	C	C	D	F	D	E	D	C	D	F	D	E	-
P5,j	D	F	D	E	C	F	C	F	E	-	-	-	-

3) Solution methodology

Five air gap MEC modules numbered as T1-T5, S1-S6, and A1-A5, respectively are used to model ORFEFSM due to its periodic nature. Repeatability of this specific 13/12 ORFEFSM allows to model only half of the machine as shown in Fig. 12. Air gap MEC modules are sensitive to rotor tooth position and results in different reluctance network topologies corresponding to change in rotor position.

Magnetic potentials of each node are computed by describing MEC modules mathematically as matrices; these matrices are merged to form GRN and solved using incidence matrix method [16] in MATLAB. Main features of incidence matrix method are explained as follows.

Incidence matrix A of a circuit having m nodes and

n branches is m x n matrix, in which:

$$A_{i,j} = \begin{cases} 1, & \text{if branch } j \text{ begins from node } i, \\ -1, & \text{if branch } j \text{ ends to node } i, \quad (3) \\ 0, & \text{if branch } j \text{ ends to node } i. \end{cases}$$

Other important variables of aforementioned m x n matrix are defined as matrix or vector as follows:

A: incidence matrix (m x n matrix),
U: mmf drop across each branch (n x 1 vector),
V: magnetic potential on each node (m x 1 vector),
E: mmf source in each branch (n x 1 vector),
Φ: flux through each branch (n x 1 vector),
R: reluctance of each branch (n x n diagonal matrix),
Λ: permeance of each branch (n x n diagonal matrix).

Following equations are derived according to Kirchhoff Circuit Laws:

$$U = A^t . V, \qquad (4)$$
$$A . \Phi = 0, \qquad (5)$$
$$U = R . \Phi + E = \Lambda^{-1} . \Phi + E. \qquad (6)$$

Equation for magnetic potential (utilizing **A**, **Λ**, and E) can be written as:

$$V = (A . \Lambda . A^t)^{-1} . (A . \Lambda . E). \qquad (7)$$

Magnetic potentials of each node are calculated by using Eq. (7) that ultimately helps to compute magnetic flux through each flux tube.

4) Validation with finite element analysis

Accuracy of nonlinear magnetic equivalent circuit models and GRN methodology for 12slot/13pole ORFEFSM is validated by comparing open-circuit phase flux linkage with corresponding FEA results. Magnetic parameters and geometric dimensions of 12slot/13pole ORFEFSM are summarized in Table 1. Comparison of open-circuit phase flux linkage obtained for GRN methodology and FEA is presented in Fig. 13. Error of open-circuit phase flux linkage between GRN methodology and FEA results is also computed and shown in Fig. 14. Results obtained from GRN methodology fairly match FEA results, as errors are less than ~1.2%, hence validating accuracy of GRN methodology.
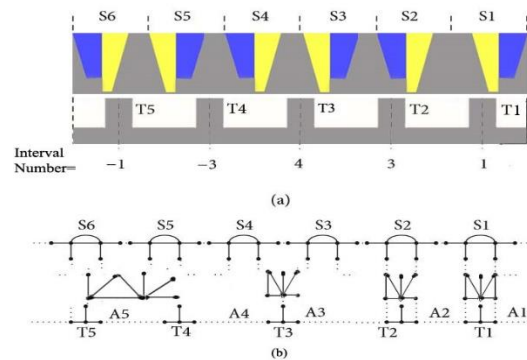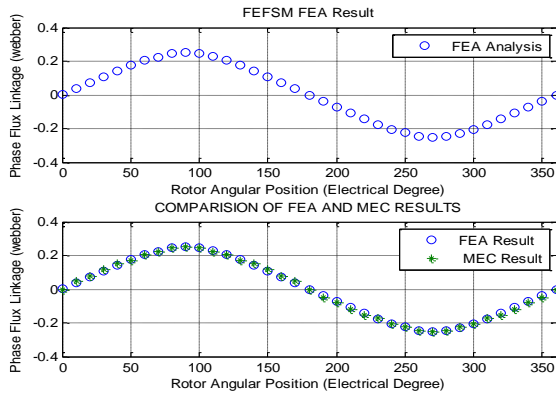

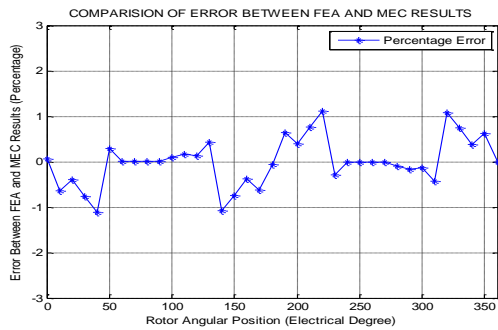Fig. 12. Global MEC of 12S-13P ORFEFSM.

Fig. 13. Combine FEA and MEC.

Fig. 14. Error between FEA and MEC.

B. Flux linkage

Figure 15 presents the magnetic flux linkage of ORFEFSM un-optimized and optimized design under the armature current density J_a is set to be 0A\mm^2 and it can be observed that the flux linkage boosted with armature current density while keeping the maximum current density of field excitation coil constant. Figure 15 depicts that highest flux linkage of optimized design is 0.252Wb and un-optimized design 0.143Wb and the optimized flux linkage 76.22 percent greater than un-optimized design.
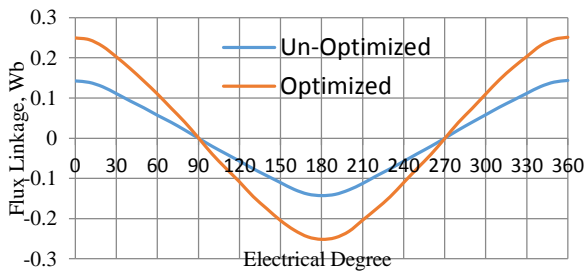

Fig. 15. U-flux lines.

C. Average electromagnetic torque

Figure 16 presents the torque verses armature current

density (J_a) curves at various armature current density keeping current density (J_e) of FEC coil constant. Figure 16 depicts the torque comparison between un-optimized and optimized design and also shows that's by increasing armature current density the torque will increased too and 0A\mm^2 to 30A\mm^2 varies armature current density and kept constant maximum field excitation coil current density and simulated the design and observed average electromagnetic torque. In comparison the optimal torque of optimized design 129.513Nm is achieved by ORFEFSM at maximum field excitation and armature current density ($J_a = J_e = 30$A\mm^2), which is approximately 45.52 percent greater than un-optimized design. One of the best advantages of FEFSM is the control the average electromagnetic torque by both armature and field current.
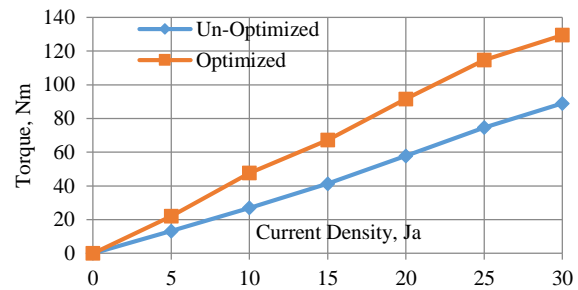

Fig. 16. Comparison of average electromagnetic torque.

D. Efficiency and losses

Figure 17, as illustrated, the efficiency, copper losses, and iron losses of the proposed design 12-slot\13-pole ORFEFSM. The copper losses are calculated from the Eq. 8 [17]:

$$Pc = \rho(2L + 2L_{end}) \times J \times I \times N \times N_{slot}. \quad (8)$$

Where L, L_{end}, and Pc is the stack length, estimated end coil length, and copper losses respectively, while N, J, N_{slot}, and I are number of turns, current density, number of stator slot, and current respectively and ρ is resistivity of copper, having 2.224×10^{-8} Ωm constant value. In Figs. 17 (a), (b) depicts the copper losses and iron losses analysis of 12-slot\13-pole ORFEFSM. The copper and iron losses decreases with employing optimization and after optimization the copper losses reduce up to 10 percent while iron losses up to 32.85 percent decreases. It's observed that the increasing armature current density also increase in copper losses and while decrease in iron losses.

The copper losses of FEC coil and armature windings are analytically determined from their geometries, by taking into consideration the end coil effect. Furthermore, the iron losses including eddy current and hysteresis losses are calculated by 2D- FEA solver providing loss data sheet of 35H210 material.
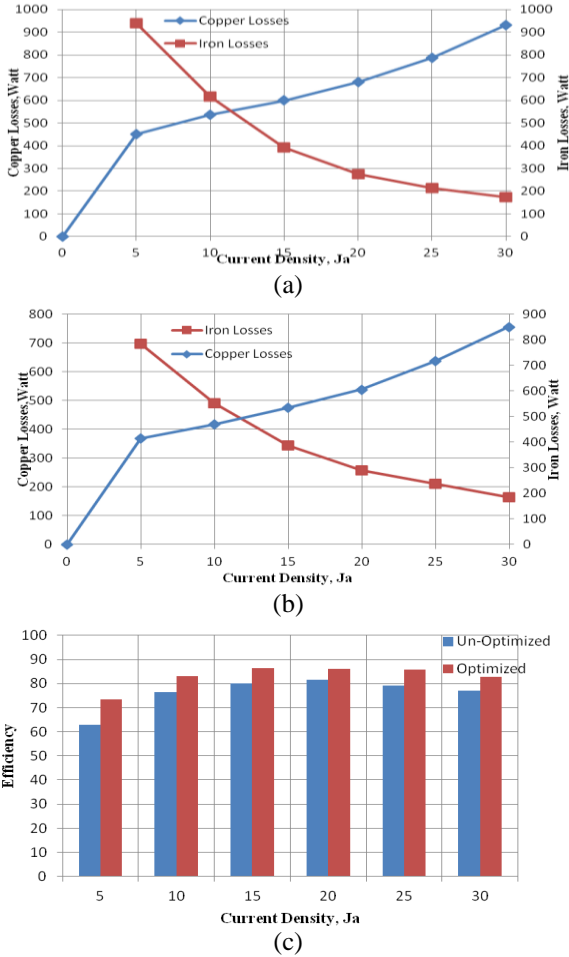
Fig. 17. (a) Copper and iron losses of un-optimized design, and (b) copper and iron losses of optimized design; (c) efficiency analysis.

Figure 17 (c) illustrates that un-optimized and optimized design efficiency bar graph between the efficiency versus the armature current J_a while keeping constant field excitation coil current density J_e. The efficiency of both designs of machine is lowest at J_a 5 A/mm^2 as presented in Fig. 17 (c). Due to less current density there are less copper losses and high iron losses due to high speed. The average efficiency of both un-optimized and optimized machine is 76.175 percent and 82.90 percent respectively and 8.2 percent efficiency of optimized design greater than un-optimized design. The copper losses are calculated form Eq. 8 and using bundle of wires. The current density at 15 A/mm^2 the machine has low speed which causes less iron losses leads to maximum efficiency. Increase in current density beyond 15 A/mm^2, copper losses increases and ultimately decrease in efficiency is observed.

IV. TORQUE COMPARISON

Figure 18 illustrates the torque verses armature current density (J_a) curves at various armature current density keeping current density (J_e) of FEC coil constant. At the highest Ja and Je of 30A\mm^2 of ORFEFSM is achieved 129.53Nm torque. As armature current density increasing torque also increase approximately linear. In the figure it compares ORFEFSM with IPM and 6-slot\7-pole NSWFS.

Internal Permanent Machine (IPM) is successfully installed and commercialized for HEV's by the Toyota Prius company. The performance parameter of IPM and 6-slot\7-pole NSWFS are published in [14]. These two machines use as bench mark. A 6-slot\7-pole NSWFS is relatively the best machine compared with other machines because of high torque density. This machine achieving approximately 60% torque density of IPM torque density at same current density. Figure 18 depicts the average torque verses current density of IPM and 6-slot\7-pole NSWFS machine [15].

The proposed motor 12-slot\13-pole ORFEFSM has been optimized to achieving maximum average torque. For performance comparison make 12-slot\13-pole motor similar size as IPM machine. The figure shows that 12-slot\13-pole ORFEFSM can achieve average torque approximately 57% of IPM and 95% of 6-slot\7-pole NSWFS.
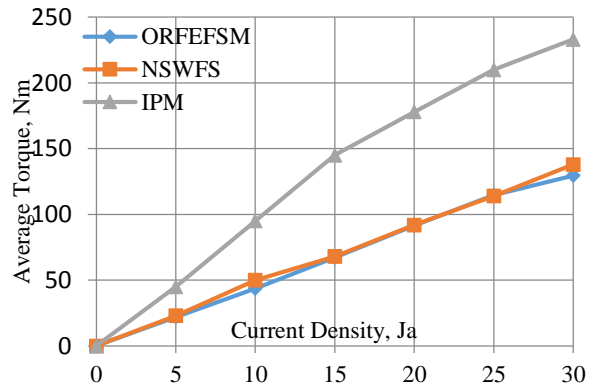

Fig. 18. Average electromagnetic torque comparison.

V. CONCLUSION

The proposed machine comprises of outer rotor, non-overlapping winding, and robust rotor structure resulting in reduced copper losses, low cost, high efficiency, and high-speed applications. The no-load and load analysis were examined to validate the efficacy of proposed machine design. Moreover, the profile of flux linkage, average electromagnetic torque, copper losses, iron losses and torque versus current density were analyzed on 2D FEA. Magnetic equivalent circuit (MEC) in air gap corresponding to different rotor positions and combined MEC models as Global Reluctance Network (GRN) and are solved utilizing incidence matrix methodology. Accuracy of nonlinear magnetic equivalent circuit models and GRN methodology for 12slot/13pole ORFEFSM is validated by comparing open-circuit

phase flux linkage with corresponding FEA results, and shows less than ~1.2% error. The initial design achieved inadequate power and torque production. Therefore, a deterministic optimization technique was adopted in this study that assisted in enhancement of power, torque, and efficiency compared to existing IPM and 6-slot\7-pole NSWFS machines.

REFERENCES

[1] W. Fei, P. C. K. Luk, J. X. Shen, Y. Wang, and M. Jin, "A novel permanent-magnet flux switching machine with an outer-rotor configuration for in-wheel light traction applications," *IEEE Transactions on Industry Applications*, vol. 48, pp. 1496-1506, 2012.

[2] J. T. Chen and Z. Q. Zhu, "Comparison of all-and alternate-poles-wound flux-switching PM machines having different stator and rotor pole numbers," *IEEE Transactions on Industry Applications*, vol. 46, pp. 1406-1415, 2010.

[3] Z. Q. Zhu and D. Howe, "Electrical machines and drives for electric, hybrid, and fuel cell vehicles," *Proceedings of the IEEE*, vol. 95, pp. 746-765, 2007.

[4] I. Boldea, C. Wang, and S. A. Nasar, "Design of a three-phase flux reversal machine," *Electric Machines & Power Systems*, vol. 27, pp. 849-863, 1999.

[5] R. P. Deodhar, S. Andersson, I. Boldea, and T. J. Miller, "The flux-reversal machine: A new brushless doubly-salient permanent-magnet machine," *IEEE Transactions on Industry Applications*, vol. 33, pp. 925-934, 1997.

[6] C. Pollock, H. Pollock, R. Barron, J. R. Coles, D. Moule, A. Court, *et al.*, "Flux-switching motors for automotive applications," *IEEE Transactions on Industry Applications*, vol. 42, pp. 1177-1184, 2006.

[7] X. Liu and Z. Q. Zhu, "Comparative study of novel variable flux reluctance machines with doubly fed doubly salient machines," *IEEE Transactions on Magnetics*, vol. 49, pp. 3838-3841, 2013.

[8] J. T. Chen and Z. Q. Zhu, "Comparison of all-and alternate-poles-wound flux-switching PM machines having different stator and rotor pole numbers," *IEEE Transactions on Industry Applications*, vol. 46, pp. 1406-1415, 2010.

[9] E. Sulaiman, T. Kosaka, and N. Matsui, "A new structure of 12slot-10pole field-excitation flux switching synchronous machine for hybrid electric vehicles," in *Power Electronics and Applications (EPE 2011), Proceedings of the 2011-14th European Conference on*, , pp. 1-10, 2011.

[10] F. Khan, E. Sulaiman, and M. Ahmad, "Coil test analysis of wound-field three-phase flux switching machine with non-overlapping winding and salient rotor," in *Power Engineering and Optimization Conference (PEOCO), 2014 IEEE 8th International*, pp. 243-247, 2014.

[11] F. Khan, E. Sulaiman, and M. Z. Ahmad. "A novel wound field flux switching machine with salient pole rotor and nonoverlapping windings," *Turkish Journal of Electrical Engineering & Computer Sciences*, vol. 25, pp. 950-964, 2017.

[12] W. Fei, P. Luk, J. Shen, and Y. Wang, "A novel outer-rotor permanent-magnet flux-switching machine for urban electric vehicle propulsion," in *Power Electronics Systems and Applications, 2009. PESA 2009. 3rd International Conference on*, pp. 1-6, 2009.

[13] Z. Q. Zhu, Y. Zhou, and J. T. Chen, "Electromagnetic performance of nonoverlapping stator wound field synchronous machine with salient pole rotor," *IEEE Transactions on Magnetics*, vol. 51, pp. 1-4, 2015.

[14] Z. Q. Zhu, Y. Zhou, J. T. Chen, and J. E. Green, "Investigation of nonoverlapping stator wound-field synchronous machines," *IEEE Transactions on Energy Conversion*, vol. 30, pp. 1420-1427, 2015.

[15] V. Ostovic, *Dynamics of Saturated Electric Machines*. Springer Science & Business Media, 2012.

[16] L. O. Chua and P. Y. Lin, *Computer-Aided Analysis of Electronic Circuits: Algorithms and Computational Techniques*. Prentice Hall Professional Technical Reference, 1975.

[17] F. Khan, E. Sulaiman, and M. Z. Ahmad, "Review of switched flux wound-field machines technology," *IETE Technical Review*, vol. 34, pp. 343-352, 2017.

Naseer Ahmad was born in 1992 in Lakki Marwat, KPK, Pakistan. He received his Bachelor degree in Electrical Power Engineering in 2015 Form UET, Peshawar, Pakistan and is currently enrolled in M.S. Electrical Power Engineering from COMSATS Institute of Information Technology, Abbottabad, Pakistan. His research interests are Optimization and Outer rotor flux switching machine.

Faisal Khan was born in Charsadda, KPK, Pakistan, on 20 June 1986. He received his B.S. and M.S. degree in Electrical Engineering from COMSATS Institute of Information Technology, Pakistan, in 2009 and 2012, respectively. He has been a Lecturer at COMSATS Institute of

Information Technology, Pakistan since 2012. He did his Ph.D. degree in Electrical Engineering at Department of Electrical Power Engineering, University Tun Hussein Onn Malaysia. His research interests include design and optimizations of wound field flux switching machines with salient rotor, Permanent magnet flux switching machines, Hybrid Excited flux switching machines and Linear Machines.

Noman Ullah is serving as Lecturer at Electrical Engineering Department, COMSATS Institute of Information Technology, Abbottabad, Pakistan. He earned B.S. in Electrical (Power) Engineering from COMSATS Institute of Information Technology, Abbottabad, and Masters in Electrical (Power) Engineering from University of Engineering & Technology, Peshawar in 2012 and 2015, respectively. His research interest includes analytical modelling and design of Permanent Magnet, Field Excited and Hybrid Excited Flux Switching Machines.

Md Zarafi Ahmad was born in Johor, Malaysia, on 11 July 1979. He received his B.E. degree in Electrical Engineering from University Technology Mara in 2003 and M.E. degree in Electrical Engineering from University Technology Malaysia in 2006. He did his Ph.D. degree in Electrical Engineering at Department of Electrical Power Engineering, University Tun Hussein Onn Malaysia. He has been Senior Lecturer at University Tun Hussein Onn Malaysia since 2006. His research interests including electrical machine and drive control.